Biol. Cybern. 91, 76–90 (2004)
DOI 10.1007/s00422-004-0498-y

Biological Cybernetics

Dynamics and stability of insect locomotion: a hexapedal model for horizontal plane motions

Justin E. Seipel[1], **Philip J. Holmes**[1,2], **Robert J. Full**[3]

[1] Department of Mechanical and Aerospace Engineering, Princeton University, Princeton, NJ 08544, USA
[2] Program in Applied and Computational Mathematics, Princeton University, Princeton, NJ 08544, USA
[3] Department of Integrative Biology, University of California, Berkeley, CA 94720, USA

Received: 23 January 2004 / Accepted: 22 June 2004 / Published online: 21 August 2004

Abstract. We develop a simple hexapedal model for the dynamics of insect locomotion in the horizontal plane. Each leg is a linear spring endowed with two inputs, controlling force-free length and "hip" position, in a stereotypical feedforward pattern. These represent, in a simplified manner, the effects of neurally activated muscles in the animal and are determined from measured foot force and kinematic body data for cockroaches. We solve the three-degree-of-freedom Newtonian equations for coupled translation-yawing motions in response to the inputs and determine branches of periodic gaits over the animal's typical speed range. We demonstrate a close quantitative match to experiments and find both stable and unstable motions, depending upon input protocols. Our hexapedal model highlights the importance of stability in evaluating effective locomotor performance and in particular suggests that sprawled-posture runners with large lateral and opposing leg forces can be stable in the horizontal plane over a range of speeds, with minimal sensory feedback from the environment. Fore–aft force patterns characteristic of upright-posture runners can cause instability in the model. We find that stability can constrain fundamental gait parameters: our model is stable only when stride length and frequency match the patterns measured in the animal. Stability is not compromised by large joint moments during running because ground reaction forces tend to align along the leg and be directed toward the center of mass. Legs radiating in all directions and capable of generating large moments may allow very rapid turning and extraordinary maneuvers. Our results further weaken the hypothesis that polypedal, sprawled-posture locomotion with large lateral and opposing leg forces is less effective than upright posture running with fewer legs.

1 Introduction

Insects can run stably over rough ground at speeds high enough to challenge the ability of proprioceptive sensing and neural feedback to respond to perturbations "within a stride". Motivated by experiments on and modeling of the cockroach *Blaberus discoidalis* as a rigid body subject to prescribed foot forces, due to Kubow and Full (1999), and by the suggestion of Brown and Loeb that, in rapid movements, "detailed" neural feedback (reflexes) might be partially or wholly replaced by largely mechanical feedback (preflexes) (Brown et al. 1995),[1] our group showed that a simple, energetically conservative model with passive elastic legs could produce asymptotically stable gaits (Schmitt and Holmes 2000a,b). This work in turn prompted experiments on rapidly running cockroaches (Jindrich and Full 2002) that strongly support the preflex hypothesis.

Our lateral leg spring (LLS) model echoes, in the horizontal plane, the passive spring-loaded inverted pendulum (SLIP) (Cavagna et al. 1977; McMahon and Cheng 1990), which has been successful in modeling saggital plane center of mass (COM) motions of a broad range of animals (Blickhan 1989; Blickhan and Full 1993). Since the insects of interest do not significantly flex their head-thorax-body and their limbs contribute only 6% of the total mass (Kram et al. 1997), in Schmitt and Holmes (2000a,b) we used a rigid body endowed with a pair of massless *effective* legs, each representing the support tripod of front, rear, and contralateral middle legs during stance in hexapedal locomotion. Each leg was placed in ground contact at a fixed extension length (corresponding to zero axial force) and fixed angle relative to the body and allowed to pivot and compress freely during the stance phase, being lifted when the force first returned to zero, at which instant the contralateral leg touched down. The legs were attached to the body at a moment-free pivot ("hip" joint), the *center of pressure* (COP), which may be fixed or allowed to move relative to the body during stance, and the foot contact point was also assumed moment-free.

Depending upon hip position or hip motion during stance, this passive model can yield stable periodic gaits.

Correspondence to: P. J. Holmes
(e-mail: pholmes@rimbaud.princeton.edu)

[1] Brown and Loeb (2000, Sect. 3) define a preflex as "the zero-delay, intrinsic response of a neuromusculoskeletal system to a perturbation", and they note that preflexes are programmable via preselection of muscle activation.

Stability derives from "angular momentum trading" as the body's support (constraint) point switches from stride to stride. An appropriate notion of stability for such piecewise-holonomic systems (Ruina 1998) is that of *partial asymptotic stability*: due to energy conservation and rotational invariance, two of the eigenvalues of the linearized Poincaré map were necessarily unity; thus, at best, the orbits were only Liapunov or neutrally stable.

In detailed parameter studies (Schmitt and Holmes 2001) and comparisons with experimental data from the cockroach *Blaberus discoidalis* (Schmitt et al. 2002), we found that, while the bipedal models of Schmitt and Holmes (2000a,b) could, with moving COP, qualitatively reproduce observed force and moment patterns, the latter in particular were an order of magnitude too low. Introducing prescribed torques and muscle actuation can produce realistic moments and yawing motions, but only at the expense of *reversing* the net fore–aft force oscillations (Schmitt and Holmes 2003). However, the addition of Hill-type activated muscle models, and dissipation characteristic of flexing joints, did not disrupt the passive stability mechanisms and added asymptotic stability with respect to forward speed (Schmitt and Holmes 2003).

In the present paper we develop a hexapedal system that combines the advantages of the Kubow–Full and bipedal LLS models, without adding much complexity. Its rudimentary representation of muscle-actuated legs driven by a stereotyped central pattern generator (CPG) reproduces forces and moments correctly while retaining the passive spring elements responsible for stability in the LLS model. Actuation is purely feedforward during each stride, the only proprioceptive signal employed being detection of zero leg force, which signals liftoff of the current stance tripod and touchdown of the next. The introduction of actuated legs and a more realistic hexapedal geometry yields a better quantitative agreement with data and is a step toward our goal of developing an integrated neuromuscular locomotion model, in which the CPG will innervate, via motoneuron models, Hill-type muscles. We believe that relatively simple models such as the present one, "templates" in the terminology of Full and Koditschek (1999), can contribute both to improved understanding of complex biological systems and to the design of bioinspired machines. See Dickinson et al. (2000) and the issue in which it is found (Chong et al. 2000) for an overview on locomotion, modeling issues, and some implications for robotics research.

This paper's contents are as follows. Section 2 describes the hexapedal model, the (idealized) foot force data (Kubow and Full 1999) used in its formulation, and the derivation of feedforward inputs that mimic muscle actuation by the CPG. In Sect. 3 we perform numerical integrations of the coupled translation/yawing dynamical equations, both at preferred speed and over a range of speeds typical of the insect. We find both stable and unstable gaits, depending upon input parameters, notably "desired" forward speed, stride frequency, and foot touchdown points, and we describe a protocol that yields stable gaits over the typical speed range employed by *Blaberus*. Section 4 develops the biological implications of this modeling study and in particular shows the possible constraints that stability imposes on fundamental gait variables, as well as the advantage of differential leg function associated with large lateral and opposing forces. We summarize and suggest future work in Sect. 5. Technical details, including those on numerical methods, are relegated to the Appendix.

We use the methods of nonlinear dynamics (Guckenheimer and Holmes 1990) in our analysis and presentation of model behavior. We refer the reader to Full et al. (2002) for an introduction to the main ideas of asymptotic stability, Poincaré maps, eigenvalues, and phase space from a biomechanical viewpoint.

2 The hexapedal model

As noted above, we wish to generalize both the simple bipedal passive and active leg spring (LLS) models of Schmitt and Holmes (2000a, 2001, 2003), in which each support tripod is replaced by a single effective leg that has either a fixed or a moving "virtual hip pivot", and the Kubow–Full hexapedal model (Kubow and Full 1999), in which forces are prescribed and unchanged by perturbations. We retain the massless, passive elastic elements responsible for stability in the simple LLS models, but move closer to biological reality and thus obtain better quantitative agreement with experiment. As in Schmitt and Holmes (2000a), to maintain simplicity, we represent each multijoint leg and its muscles by a single telescoping unit that supports only axial forces but whose unstressed length, $l(t)$, and attachment point ("hip", or body-coxa joint) relative to mass center, $d(t)$, are prescribed functions of time. Thus each leg has two *inputs*, representing the coordinated effects of muscle contractions driven by motoneurons excited by the insect's central pattern generator, that allow us to match experimentally observed foot force magnitudes and directions. (Instead of a moving hip, one could supply torques at a fixed pivot via a torsional spring, but the moving hip protocol seems simpler, and moreover exploratory studies with torsional springs did not yield any stable gaits, as noted at the end of Sect. 3.2. Implications for moments produced by individual legs, discussed in Sect. 4.3, are similar in both cases.)

While this strategy may be generalized to other hexapods and multilegged animals, it is applied here to the death's head cockroach *Blaberus discoidalis* running in a double-tripod gait at its preferred speed, and parameters specific to that insect are used. The experimental data of Full and Tu (1990), Full et al. (1991), and Ting et al. (1994) include individual leg (vector) forces and positions of the feet at touchdown; from these, following Kubow and Full (1999) and employing simplifying assumptions, we derive in a self-consistent manner typical forces and body motions throughout the left and right tripod stance phases. The six horizontal plane force components at each support tripod, with some planar kinematics, then yield the six required inputs.

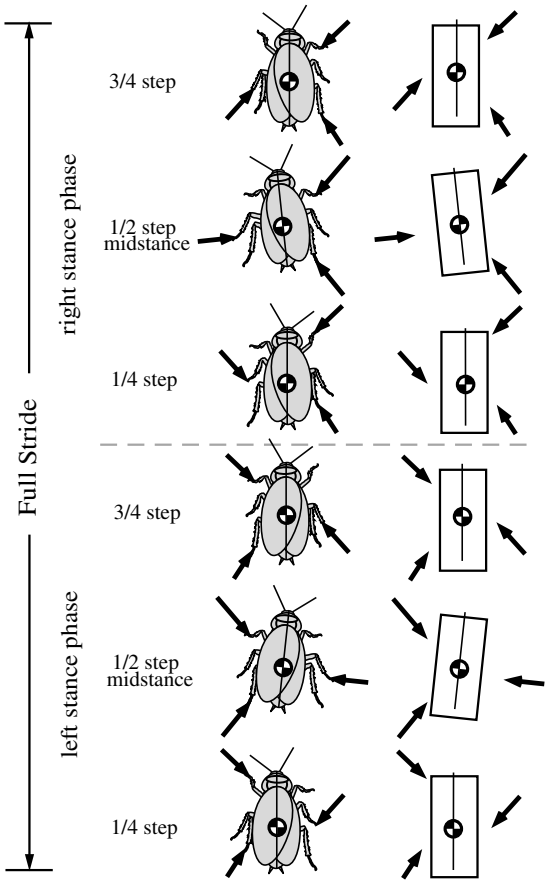

Fig. 1. The double-tripod gait and a mechanical realization as a triad of prescribed forces applied to a planar rigid body, from Kubow and Full (1999)

2.1 Insect data

Figure 1 shows the typical double-tripod gait exhibited by many hexapedal runners. Figure 2 shows the mechanical model, body and inertial coordinate systems, and leg numbering scheme. The legs numbered 1, 2, and 3 comprise the *left stance tripod* and correspond to the legs on the ground during the first stance phase in Fig. 1, also called the left stance phase or half-stride. Likewise, legs 4, 5, and 6, the *right stance tripod*, correspond to those on the ground for the second half-stride. Figure 3 shows sinusoidal approximations of filtered and averaged forces observed during experiments (Full and Tu 1990, 1991; Full et al. 1991; Ting et al. 1994), as derived in Kubow and Full (1999), given in the inertial frame $(\mathbf{e}_x, \mathbf{e}_y)$, with the animal running at its preferred speed in the y-direction (as we shall see, its COM and body orientation oscillate slightly about the purely straight path). These take the forms:

$$\begin{aligned} F_{ix} &= A_{ix} \sin \Omega t\,, \ i = 1, \ldots, 6\,, \\ F_{iy} &= A_{iy} \sin \Omega t\,, \ i = 1, 3, 4, 6\,, \\ F_{iy} &= A_{iy} \sin 2\Omega t\,, \ i = 2, 5\,, \end{aligned} \tag{1}$$

where Ω denotes the leg cycle or stride frequency (in rad/s^{-1}). Table 1, also adapted from Kubow and Full (1999), summarizes geometrical and biomechanical data, including foot touchdown positions relative to COM in body coordinates, to be used below.

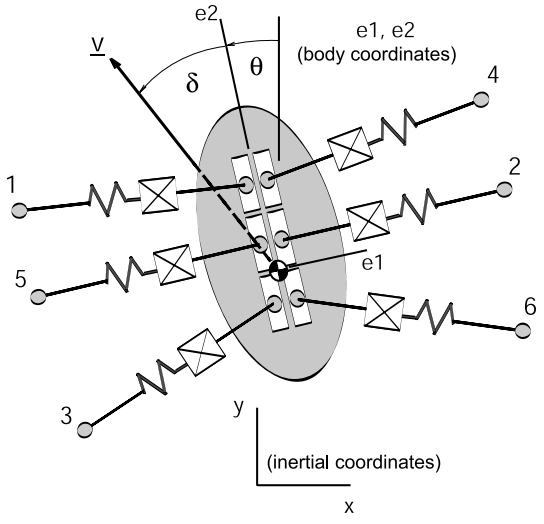

Fig. 2. The coordinate systems and leg numbering scheme

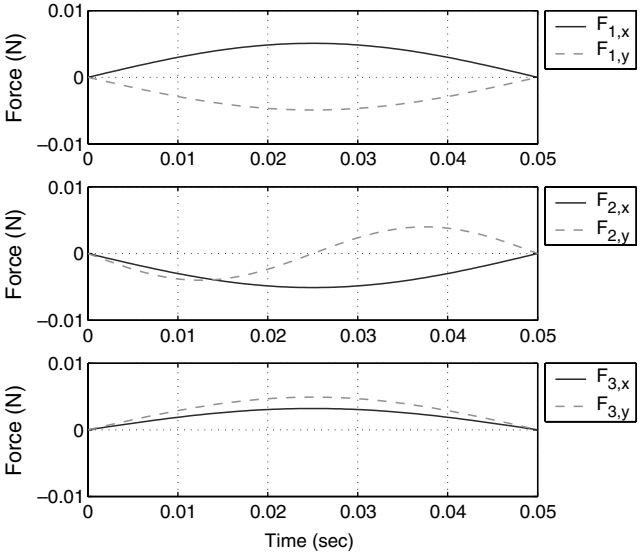

Fig. 3. Sinusoidal idealizations of observed leg forces: $F_{jx} = A_{jx} \sin \Omega t$; $F_{jy} = A_{jy} \sin \Omega t$, $j = 1, 3$; $F_{2y} = A_{2y} \sin 2\Omega t$. From Kubow and Full (1999)

2.2 Actuation, liftoff, touchdown, and other assumptions

Figure 4a shows a mechanical realization of the leg model. Moment-free pivots are assumed at the foot, which is fixed in the inertial frame during stance, and at the (virtual) hip, which moves along the body centerline. The spring is assumed linear and the legs massless. Actuators adjust the unstressed leg lengths $l_i(t)$ and hip position relative to the COM $d_i(t)\mathbf{e}_2$, so that the axial force developed in each leg is

$$F_i = k_i(l_i(t) - |\mathbf{q}_i|)\,, \tag{2}$$

where $|\mathbf{q}_i|$ is total leg length. Left stance begins with legs 1–3 placed with their feet at the touchdown points of Table 1 and ends when the first of the forces $F_i, i = 1, 2, 3$ drops to zero, at which instant legs 1–3 are raised, legs 4–6 touch down at their appointed (laterally symmetric)

Table 1. Cockroach parameters: adapted from Kubow and Full (1999)

Parameter	Value
Body mass (m)	0.0025 kg
Moment of inertia about vertical axis (I)	2.04×10^{-7} kg m^2
Stride frequency ($f = \Omega/2\pi$)	10 Hz
Preferred fore–aft velocity (V_{pref})	0.25 m sec^{-1}
Foot touchdown in body coords (e_1, e_2)	
$\mathbf{b}_1$, front left foot	$(-0.011, +0.02)$ m
$\mathbf{b}_2$, middle right foot	$(+0.013, +0.007)$ m
$\mathbf{b}_3$, hind left foot	$(-0.013, -0.01)$ m
$for\ i = 1..3,\ b_{i+3,e1} = -b_{i,e1}$ and $b_{i+3,e2} = b_{i,e2}$	
Force Magnitude (inertial x-component)	
A_{1x}, A_{4x} front legs	$+0.0051, -0.0051$ N
A_{2x}, A_{5x} middle legs	$-0.0051, +0.0051$ N
A_{3x}, A_{6x} hind legs	$+0.0032, -0.0032$ N
Force Magnitude (inertial y-component)	
A_{1y}, A_{4y} front legs	$-0.0049, -0.0049$ N
A_{2y}, A_{5y} middle legs	$-0.0040, -0.0040$ N
A_{3y}, A_{6y} hind legs	$+0.0049, +0.0049$ N

positions, and the right stance phase begins. Thus the duty cycle is 50%, compared to 55–65% in the insect (Ting et al. 1994, Fig. 3). This protocol models the CPG-driven muscles and includes minimal proprioceptive feedback.

These simplifications and assumptions are listed in Table 2. To complete the model prescription, in the next subsection we deduce appropriate actuation inputs $l_i(t)$, $d_i(t)$. While two inputs per leg are required to match the two-component (horizontal) force vector measured at each foot, choices other than the present ones are possible. For example, hip positions could be fixed and adjustable torques applied at each hip either directly or via a torsional spring with adjustable "zero-moment" angle. We shall briefly comment on such protocols in our discussions of stability in Sect. 3.2.

2.3 Derivation of actuation inputs

The inputs should produce the same forces as those generated at the insect's feet during the ideal (desired) motion: Table 1 and Fig. 3. The functions $l_i(t)$ and $d_i(t)$ are therefore found by observing that the force components in the individual legs of each tripod must sum to produce the total force vector responsible for the desired body motion. This ultimately results in two equations per leg that can be solved uniquely for l_i and d_i, as we now show.

Table 2. Simplifications and assumptions

Rigid body model only moves in horizontal (lateral) plane
Model moves with alternating tripod gait, 50% duty cycle
Feet stay fixed in inertial space during stride
Stance phase ends and all three feet lift when any leg force = zero
Legs are assumed massless and springs linear
Hip pivots move along body centerline
Yawing motions are neglected in solving for inputs (Sect. 2.3)

Bilateral symmetry implies that leg parameters reflected across the body centerline must be equal:

$$\begin{aligned} &d_{i+3}(t - t_R) = d_i(t - t_L) \quad \text{and} \\ &l_{i+3}(t - t_R) = l_i(t - t_L), \quad i = 1, 2, 3, \end{aligned} \tag{3}$$

where t_L and t_R denote touchdown instants for succeeding left and right stance phases. It therefore suffices to derive inputs for one tripod, here the left: legs 1, 2, and 3. Force consistency requires that:

$$F_{ix} = F_{ix,\text{desired}} \Rightarrow k_i(l_i(t) - |\mathbf{q}_i|)\frac{q_{ix}}{|\mathbf{q}_i|} = A_{ix} \sin \Omega t\,, \tag{4}$$

$$F_{iy} = F_{iy,\text{desired}} \Rightarrow k_i(l_i(t) - |\mathbf{q}_i|)\frac{q_{iy}}{|\mathbf{q}_i|} = A_{iy} \sin C_i \Omega t\,, \tag{5}$$

where q_{ix} and q_{iy} are the inertial frame components of q_i and A_{ix} and A_{iy} the force component magnitudes of (1) (note $C_i = 2$ for $i = 2$, but $C_i = 1$ otherwise).

The components q_{ix} and q_{iy} can be written in terms of the COM path $\mathbf{r}(t) = (x(t), y(t))$, and $d_i(t)$. From the vector representation of Fig. 4b, $\mathbf{q}_i = \mathbf{r} + \mathbf{d}_i - \mathbf{p}_i$, or:

$$\begin{aligned} q_{ix} &= x(t) - d_i(t)\sin\theta(t) - p_{ix}\,, \\ q_{iy} &= y(t) + d_i(t)\cos\theta(t) - p_{iy}\,, \end{aligned} \tag{6}$$

where p_{ix} and p_{iy} are formed from the ith foot touchdown location in body coordinates, given in Table 1 as the vector $\mathbf{b}$; hence:

$$\begin{aligned} p_{ix} &= b_{i,e1}\cos\theta(t) - b_{i,e2}\sin\theta(t) + x(t_L)\,, \\ p_{iy} &= b_{i,e1}\sin\theta(t) + b_{i,e2}\cos\theta(t) + y(t_L)\,, \end{aligned} \tag{7}$$

and the COM position appears in q_{ix}, q_{iy} only in the *relative* distances $x(t) - x(t_L)$ and $y(t) - y(t_L)$. This translation invariance will be important later, when we reduce the problem to study of a four-dimensional "full-stride map".

To solve (4–7) for $d_i(t)$ and $l_i(t)$ requires the COM path $\mathbf{r}(t)$, which may be found by integrating the total forces on and moments about the COM twice and applying appropriate initial conditions. However, the moments in turn depend upon the path and so we simplify by decoupling rotational motions using the fact that yaw (θ) variations are small ($\pm 5^\circ$ Ting et al. 1994; Kubow and Full 1999) to justify approximation of the rotation matrix implicit in (6) and (7) by the identity. By thus ignoring yawing and setting $\theta(t) \equiv 0$, we effectively approximate the force components in the inertial frame by those in the body frame. We may then solve explicitly for $\mathbf{r}(t)$ by simply integrating Newton's equations for the COM translation dynamics:

$$\begin{aligned} m\ddot{\mathbf{r}} &= \mathbf{F}, \quad \text{with} \quad \mathbf{F} = (F_x, F_y) \\ &= \left(\sum_{i=1}^{3} A_{ix} \sin \Omega t, \sum_{i=1}^{3} A_{iy} \sin C_i \Omega t \right). \end{aligned} \tag{8}$$

Choosing the constants of integration to obtain periodic motions in the x direction and the preferred average speed in the y direction, and using the fact that certain force components cancel (Table 1), this yields:

$$\begin{aligned} (x(t), y(t)) = \Big(&-A_{3x}(m\Omega^2)^{-1} \sin \Omega t, \\ &-A_{2y}(4m\Omega^2)^{-1} \sin 2\Omega t + V_{\text{des}} t \Big)\,, \end{aligned} \tag{9}$$

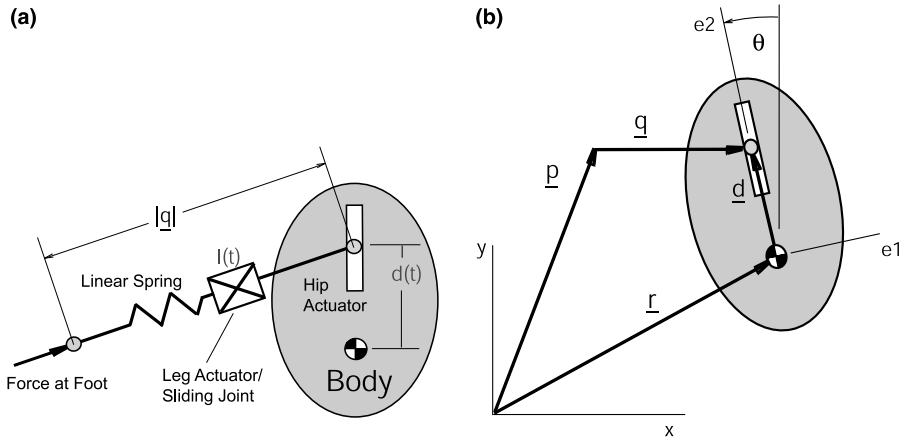

Fig. 4. Mechanical model for a single leg (**a**) and kinematics (**b**)

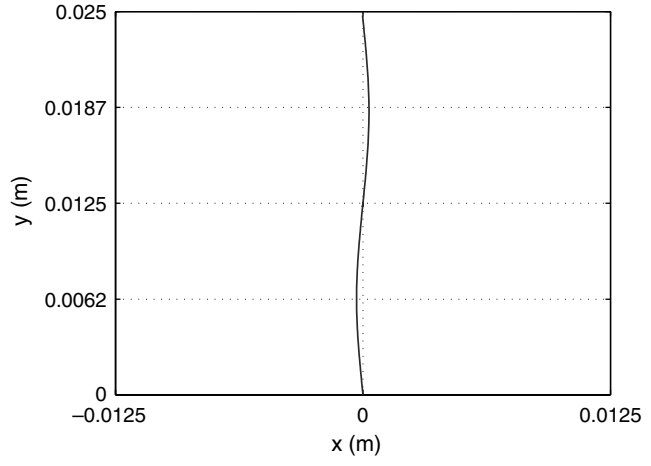

Fig. 5. The nominal COM path of (9), computed neglecting yawing

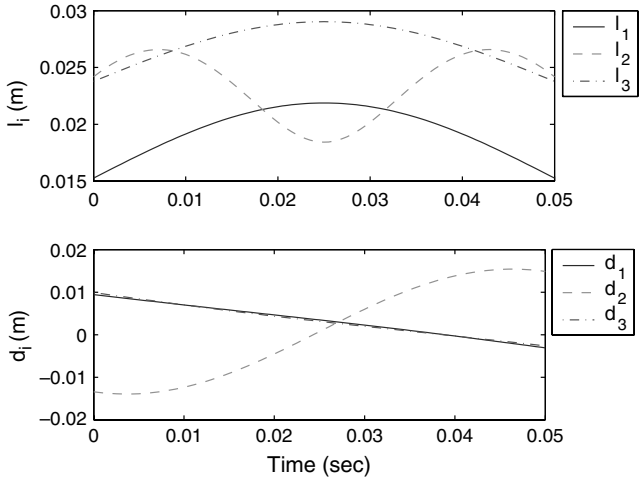

Fig. 6. The prescribed inputs, $d_i(t)$ and $l_i(t)$, for $i = 1, 2, 3$; $V_{\text{des}} = V_{\text{pref}} = 0.25\,\text{ms}^{-1}$, $\Omega = 20\pi$ rad/s^{-1} and $k = 1$ Nm

where we take $t_L = 0$ and denote the desired average forward speed by V_{des}, rather than V_{pref} (Table 1), since we will ultimately wish to vary V_{des} to produce gaits over the animal's entire speed range. The resulting path, with $V_{\text{des}} = V_{\text{pref}}$, is shown in Fig. 5.

To solve for $d_i(t)$ we divide (4–5) and use (6–7) with $\theta \equiv 0$ to write:

$$y(t) + d_i(t) - p_{iy} = [x(t) - p_{ix}]\frac{F_{iy}}{F_{ix}}$$

$$\Rightarrow d_i(t) = b_{i,e2} - y(t) + (x(t) - b_{i,e1})\left[\frac{A_{iy}\sin C_i\Omega t}{A_{ix}\sin\Omega t}\right]. \quad (10)$$

Finally, $l_i(t)$ is found by inverting (2):

$$l_i(t) = \sqrt{q_{ix}^2 + q_{iy}^2} + \frac{1}{k}\sqrt{A_{ix}^2\sin^2\Omega t + A_{iy}^2\sin^2 C_i\Omega t}\,, \quad (11)$$

and substituting for q_{ix} and q_{iy} using (6–7) with $\theta \equiv 0$. Thus the six inputs are uniquely determined by the six foot-force components. We note that the spring law does not enter until the final step [it does not influence the pivot positions $d_i(t)$] and that a similar analysis will apply to a nonlinear spring, provided that the force law can be inverted.

Figure 6 shows $d_i(t)$ and $l_i(t)$ for $i = 1, 2, 3$, with the spring constant k set at 1 Nm. Increases in k would lead, via (11), to decreases in $l(t)$. The unstressed lengths on average obey $l_1 < l_2 < l_3$, echoing leg lengths in the insect. Also, the front and back (ipsilateral) hips move backward relative to the body during stance, while the middle (contralateral) hip moves forward. The latter varies by over 3 cm, a greater distance than the insect's body length. We recall that these moving centers of pressure imply torques at the animal's (fixed) joints: thus this model suggests that the insect generates middle-leg torques larger than those of the front and hind legs.

3 Dynamical behavior

Equipped with actuation inputs that produce a self-consistent periodic gait in the absence of body rotation, we now integrate the coupled translation-rotation equations of Newtonian planar rigid body dynamics through each stance phase:

$$m\ddot{\mathbf{r}} = \mathbf{F},\ I\ddot{\theta} = \mathbf{M}. \quad (12)$$

Here $\mathbf{F}$ denotes the sum of the force vectors, in the inertial frame, for each foot of the current stance tripod, and $\mathbf{M}$ denotes the summed moments about the COM due to

those forces; specifically, from the relations developed in Sect. 2, we have:

$$F_{ix} = k_i(l_i(t) - |\mathbf{q}_i|)\frac{q_{ix}}{|\mathbf{q}_i|},\ F_{iy} = k_i(l_i(t) - |\mathbf{q}_i|)\frac{q_{iy}}{|\mathbf{q}_i|},$$
$$M_i = -\frac{d_i(t)F_i}{|\mathbf{q}_i|}(q_{ix}\cos\theta + q_{iy}\sin\theta), \qquad (13)$$

where $|\mathbf{q}_i| = \sqrt{q_{ix}^2 + q_{iy}^2}$ and q_{ix} and q_{iy} are determined from (6) and (7).

Along with the stance switching protocol defined in Sect. 2.2 (Table 2), (12) and (13) define a *hybrid dynamical system* (Guckenheimer and Johnson 1995). The "final conditions" $(x(t_{LO}), y(t_{LO}), \theta(t_{LO}), \dot{x}(t_{LO}), \dot{y}(t_{LO}), \dot{\theta}(t_{LO}))$ at the end of each stance phase become the initial conditions for the next, and the appropriate foot placement parameters $b_{i,ej}$ (Table 1) are applied for the new tripod. As noted in Sect. 2.2, t_{LO} is determined by the first leg force F_i that drops to zero.

Although the time-dependent inputs are prescribed, due to the rotational coupling these equations are nonlinear and insoluble in closed form. Below we use direct numerical simulation of an initial value problem and use such simulations to define full-stride Poincaré maps (Guckenheimer and Holmes 1990) and numerical linearization to compute the Jacobian and hence find eigenvalues that characterize stability. We start with direct simulations. For the first runs reported below, we use the inputs $l_i(t), d_i(t)$ derived from data of Table 1 at the insect's preferred velocity; subsequently we will derive inputs appropriate for running throughout the animal's typical speed range.

3.1 Stable running at preferred speed

Using the Runge–Kutta algorithm `ode45` within MATLAB, we first integrated (12) and (13) with very large I to check that the "design" COM path of Fig. 5 was produced and then reduced to the physically relevant $I = 2.04 \times 10^{-7}$, finding the steady gait illustrated in Fig. 7. The force and velocity components are close to those of the idealized insect. More strikingly, direct comparisons with nonaveraged data shown in Fig. 8 confirm that the model reproduces rather well both translation and rotation dynamics of insects running at preferred speed. We note, however, that the full, coupled dynamics results in a different average forward speed from the desired speed V_{des} used in derivation of the inputs (here, $0.26\,\text{ms}^{-1}$ compared to $0.25\,\text{ms}^{-1}$).

We now illustrate that the gaits found above are partially asymptotically stable in the sense noted in the introduction by applying discrete perturbations in COM velocity and body angle and body angular velocity. In each case, after establishing a stable gait with average direction of motion along the y-axis, we doubled one of the four touchdown conditions $(\theta(t_L), \dot{x}(t_L), \dot{y}(t_L), \dot{\theta}(t_L))$ and continued integrating. Figures 9 and 10 show examples of the results, with COM paths shown and solutions also projected onto the (V_{e1}, V_{e2})-phase plane to show how the

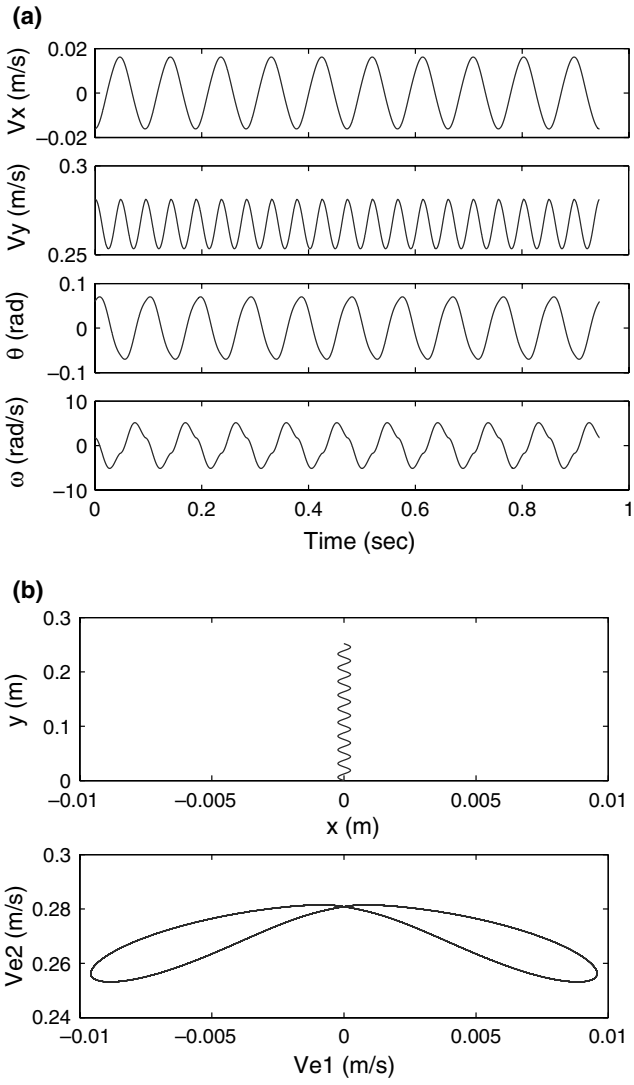

Fig. 7. **a** COM lateral (V_x) and fore–aft (V_y) velocities, yaw angle (θ), and body angular velocity (ω) vs. time for the hexapedal model running in a steady gait at preferred speed. **b** COM path in the (x, y)-plane and COM velocity components (V_{e1}, V_{e2}) in the body frame

gait returns to a stable limit cycle in "internal" body coordinates, while drifting with respect to heading angle (θ) but returning to a straight path.

3.2 Running over a range of speeds: Poincaré maps and stability

Equations (10 and 11) reveal that the desired speed V_{des}, which appears in the expression for the COM path (9), influences the inputs. A simple way to produce gaits over a range of speeds is, therefore, to recompute $l_i(t)$ and $d_i(t)$ for various V_{des}. We did this for the range 0.1–$0.6\,\text{ms}^{-1}$, typically employed by *Blaberus* (Ting et al. 1994). To better characterize the resulting gaits, we defined a full-stride (left tripod touchdown to next left tripod touchdown) Poincaré map by assembling numerical solutions of (12) and (13) for many initial (touchdown) conditions and solved for fixed points by a Newton–Raphson scheme,

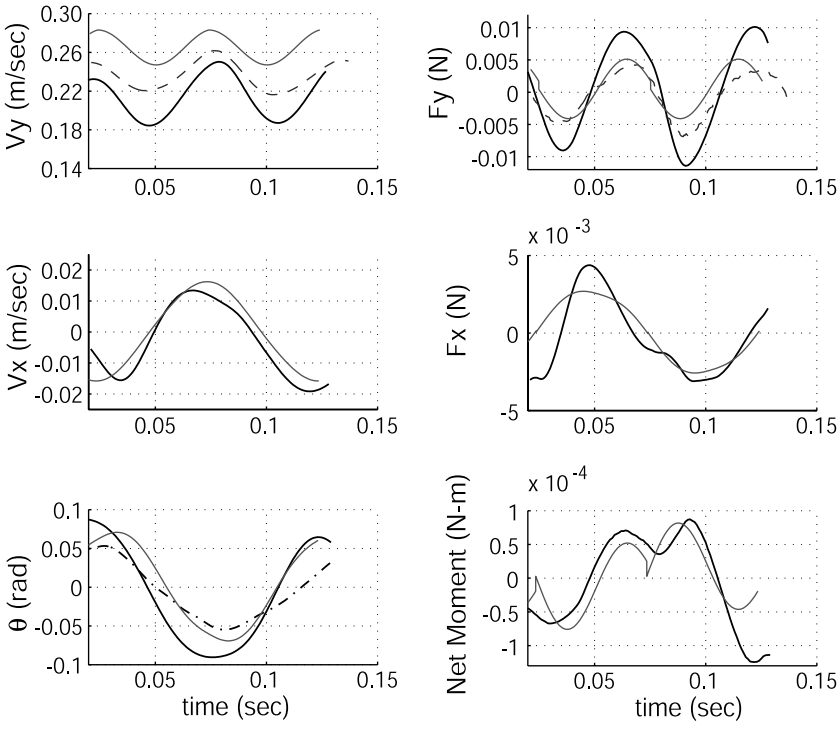

Fig. 8. Comparison of insect data with the LLS Hexapod model. Fore–aft and lateral force (F_y, F_x) and velocity (V_y, V_x), moment and yaw (θ) data from a single trial on *Blaberus discoidalis* (Full et al. 1991; Kram et al. 1997) are shown as *dark solid curves*. The corresponding yaw angle variation is computed by integrating the net moment. Yaw variations directly measured by observing the insect are shown *dashed-dotted*. For the fore–aft velocity and force components, a second set of data from a different trial (Full and Tu 1990) (*dashed*) is included to illustrate trial-to-trial variation in magnitudes and average speed. See Schmitt et al. (2002) for more information on data derivation. The model solutions are shown as a *red* (or *light gray*) *solid line*

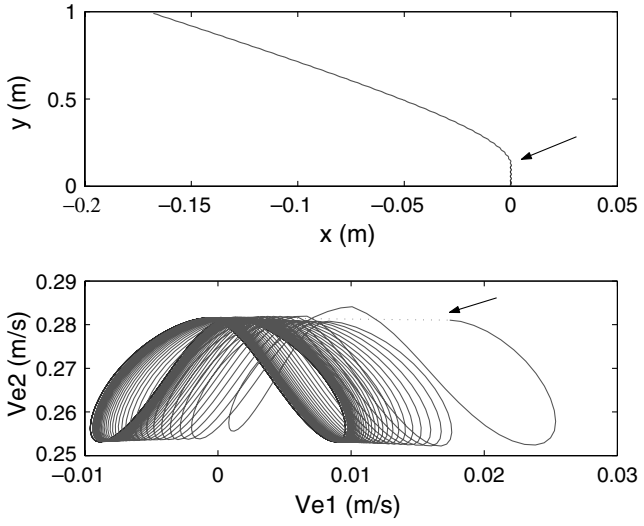

Fig. 9. Trajectory in the (x, y)-plane and (V_{e1}, V_{e2}) body coordinate phase plane for a perturbation in θ, applied at point indicated by *arrows*

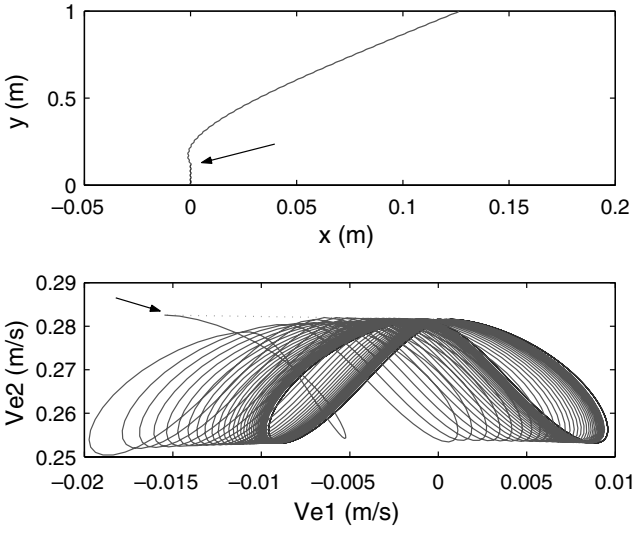

Fig. 10. Trajectory in the (x, y)-plane and (V_{e1}, V_{e2}) body coordinate phase plane for a perturbation in $\dot{x}$, applied at point indicated by *arrows*

much as in earlier bipedal studies (Schmitt and Holmes 2000a). As in that work, we introduce new coordinates: $v =$ COM velocity magnitude, $\delta =$ COM velocity vector angle with respect to body frame, retained $\theta =$ angular orientation of body in inertial frame, and $\omega = \dot{\theta} =$ angular velocity of body (Fig. 2). Letting $\mathbf{x}_k = (v_k, \delta_k, \theta_k, \omega_k)$, where k denotes the kth left tripod touchdown, the full stride Poincaré map thus takes the form:

$$\mathbf{x}_k \mapsto \mathbf{P}(\mathbf{x}_k) = \mathbf{x}_{k+1}\,, \tag{14}$$

and a fixed point $\mathbf{P}(\mathbf{x}^*) = \mathbf{x}^*$ of $\mathbf{P}$ corresponds to a steady (periodic) "straight gait".

We note that these four variables suffice to characterize the body's dynamical state at touchdown and that all six initial conditions needed for integration of (12) and (13) can be found from them using the leg placement vectors $\mathbf{b}_{i,ej}$ and the fact that, within stride, the dynamics depends upon the *difference* between the COM location and the foot positions [cf. (6) and (7)]. Effectively, as far as the intrinsic body dynamics is concerned, the COM location may be reset to (0, 0) at each touchdown.

We then approximated the linearized Poincaré map as a 4×4 matrix:

$$[\mathbf{DP}]_{ij} = \frac{\partial P_i}{\partial x_j} \tag{15}$$

via the same finite difference method used in (Schmitt and Holmes 2000a) and computed its eigenvalues at the fixed points found above. See the appendix for details of numerical methods. Linearized stability theory for maps (Guckenheimer and Holmes 1990; Full et al. 2002) states that if any eigenvalue has modulus greater than one, the fixed point is unstable: almost all neighboring solutions diverge from it as time progresses. If all eigenvalues have moduli less than one, the fixed point is asymptotically stable: all solutions starting sufficiently close approach it as time progresses. However, complete asymptotic stability is impossible here: the system is rotation invariant and there is no mechanism for sensing heading; hence, to the internal dynamics all θ angles are equal.[2] This implies that the eigenvalue associated with rotational perturbations (λ_4) is necessarily unity, corresponding to neutral stability with respect to such perturbations, as illustrated in Fig. 11. The fact that the eigenvalues found below include one that remains unity throughout (within an error of 0.005%) serves as a check on numerical accuracy.

We first held the leg cycle frequency $f = \Omega/2\pi$ fixed at 10 Hz and varied only V_{des}, producing the branch of gaits illustrated in the left column of Fig. 11. In the upper panels the abcissa represents the true forward speed $< v >$, computed as stride length divided by stride period, rather than the COM velocity ($v = \sqrt{\dot{x}^2 + \dot{y}^2}$). While stable periodic gaits corresponding to a fixed point of $\mathbf{P}$ persist above the preferred speed, as speed is reduced to about 0.24 ms^{-1}, the straight gait destabilizes in a pitchfork bifurcation, and two new stable solutions, corresponding to running in (large) circles, emerge, as shown in Fig. 12. They subsequently recollapse onto the straight gait, which restabilizes in a second pitchfork bifurcation at approximately 0.15 ms^{-1}.

Instability at lower speeds is perhaps not surprising since the insect substantially varies its stride frequency, particularly in the range 0.05–0.3 ms^{-1}; at higher speeds, stride frequency approaches $\approx$ 13 Hz, and the animal runs faster by increasing its stride length. The top panels of Fig. 11 reproduce data points from (Ting et al. 1994, Fig. 2) illustrating this. We therefore repeated our derivation of inputs over the range 0.1–0.6 ms^{-1}, appropriately varying Ω. We first increased Ω throughout the entire speed range, matching the data below 0.35 ms^{-1} but continuing linearly thereafter (Fig. 11d). As shown in the second column of Fig. 11, the resulting gaits are stable at low speeds but unstable above 0.35 ms^{-1}. We then varied Ω to better approximate the data throughout, increasing it linearly with V_{des} up to 0.35 ms^{-1}, and holding it fixed thereafter, as indicated by the piecewise-linear relation of Fig. 11g. This yields the branch of gaits shown in the third column of Fig. 11, in which stability is preserved throughout the entire speed range, although one eigenvalue almost reaches unit magnitude at about 0.35 ms^{-1} (Fig. 11i).

Stride lengths necessarily increase with increasing speed when frequency is held constant, so unless foot touchdown locations are *also* allowed to change, foot liftoff positions move further and further backwards relative to the COM location. This leads to static instability as the COM begins to fall outside the tripod defined by the stance feet at high speeds (cf. Ting et al. 1994, Fig. 1) and also implies unrealistically large rearward leg extensions. It is natural, therefore, to further modify our model touchdown protocol as stride length increases to place feet further forward at touchdown, thus maintaining the approximate symmetry that puts the COM near the centroid of the support tripod at midstance. This can be achieved either by increasing the magnitude of the vector from the hip to the foot touchdown position (i.e., further extending the leg) or by decreasing the angle between the leg and body axis at touchdown, and we chose a combination of these that effectively limits the maximal leg extension to $\pm 50\%$ of its relaxed length at $V_{\text{des}} = 0.25$ ms^{-1}. Touchdown positions were left at the nominal ones given by $\mathbf{b}_j$ of Table 1 for $V_{\text{des}} \leq 0.25$ and varied linearly with V_{des} for $V_{\text{des}} > 0.25$, placing the feet further forward and out relative to the body, as detailed in the appendix. This yields the fourth column of Fig. 11.

The lack of kinematic data over a range of speeds does not allow us to confirm that the insect does precisely this, although we do know that its COM moves backward relative to the support triangle and falls outside it at the highest speeds (Ting et al. 1994). For simplicity, both our frequency and touchdown protocols are piecewise linear with respect to V_{des}, while the experimental data indicates a "smoother" relationship (Fig. 11, top panels). In choosing $V_{\text{des}} = 0.25$ and $V_{\text{des}} = 0.35$ respectively as breakpoints for the touchdown and frequency protocols, we have bracketed the speed range in which the insect transitions from employing frequency increase to stride length increase, and we believe that this combined variation of frequency and touchdown positions with speed is biologically realistic.

As column IV of Fig. 11 shows, this final protocol further enhances stability, in particular reducing the magnitude of the largest eigenvalue within the unit circle in the 0.2–0.4 ms^{-1} speed range (Fig. 11, panel l). In all four cases, at the high-speed end, a pair of complex conjugate eigenvalues approaches the unit circle, indicating incipient destabilization in a Hopf bifurcation (Guckenheimer and Holmes 1990). We remark that similar bifurcations occur for increasing speed in the bipedal model for small moments of inertia (Schmitt et al. 2002, Sect. 5). At the low-speed end ($\approx$ 10 ms^{-1}), for the variable-fequency protocols, a second pair of eigenvalues also approaches the unit circle (Fig. 11f,i,l).

We end this section by observing that exploratory studies of the prescribed torque and preferred torsional spring angle input protocols, noted in Sect. 2.2 as possible alter-

[2] Body angle θ appears in the kinematic description relating body to inertial coordinates, but at each touchdown, like COM position, it could be reset to 0 without affecting the internal dynamics of the succeeding stride. Of course, to compute the COM path in physical space, we must maintain a record of x, y and θ from stride to stride.

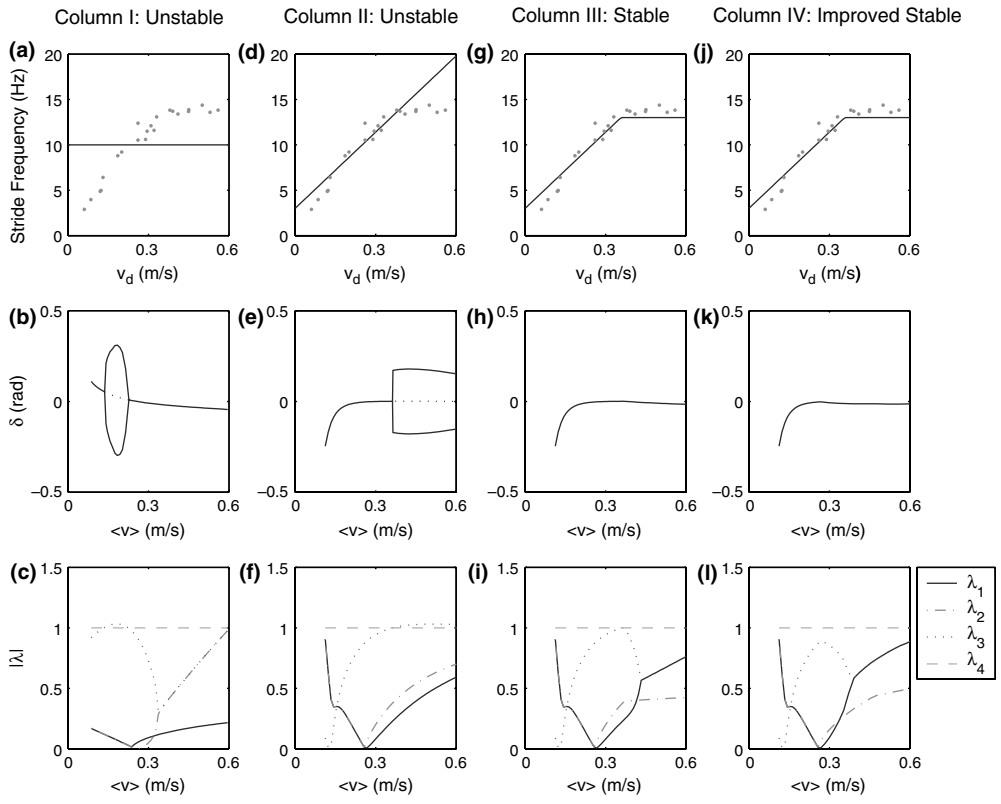

Fig. 11. Stability properties of the model over a range of forward speeds. To produce column I V_{des} alone is varied; for columns II–IV V_{des} and Ω are simultaneously varied as described in Sect. 3.2 and pictured in *top panels* (**a, d, g**) and (**j**), which also show experimental frequency/speed data from Ting et al. (1994). For column IV foot placements $\mathbf{b}_j$ are additionally varied as described in Sect. 3.2. **b**, **e**, **h**, **k** Bifurcation diagrams as COM velocity angle δ vs. "true" forward speed $< v >$. **c**, **f**, **i**, **l** Eigenvalue magnitudes of linearized Poincaré map vs. true speed. Note that the eigenvalue λ_4, corresponding to rotational perturbations, remains unity throughout; see text

natives to varying hip position $d_i(t)$, yielded *no* stable gaits (although we did find periodic gaits with appropriate foot forces and COM moments). In the case of prescribed torques and hips coincident with the COM, it is clear that the rotational equation entirely decouples as $I\ddot{\theta} = M(t)$, which may be integrated directly, leading to a double unity eigenvalue for the linearized stride map and unstable "drifting" solutions in which the body angular velocity remains constant. In general, however, while other forms of translation-rotation coupling *could* result in stability, our simulations suggest that this is not common, in contrast to the present, relatively robust $l_i(t), d_i(t)$ protocol. We do not at present have any "mechanical" intuition on this finding, although we note that in other mechanical problems similar solutions may display very different stability properties when subject to perturbations that satisfy different constraints (Maddocks 1984, 1987).

4 Implications for biology

Animals that run over rough or inclined terrain and are perturbed by wind, debris, and predators benefit from a low center of mass and a sprawled posture. Legs sprawled in all directions increase stabilizing moments that mitigate overturning (Ting et al. 1994). However, given a many-legged, sprawled-posture design, rapid forward locomotion appears to be a challenge. Sprawled-posture runners exhibit differential leg function. Legs on the left produce large lateral ground reaction forces, accelerating the body to the right, while right legs accelerate to the left (Full et al. 1991). In insects, forward-projecting (front) legs develop decelerating forces that oppose forward motion during a step, while hind legs accelerate the COM in the direction of motion. Middle legs operate more like a pivoting spring, first decelerating and then accelerating the COM during each step. Surprisingly, the summed behavior of individual legs can be described by a mass attached to a single virtual leg spring bouncing up and down in the sagittal plane (SLIP) (Blickhan and Full 1993) and side to side in the horizontal plane (LLS) Schmitt and Holmes (2000a,b). Even more startling is the fact that these simple models can show passive dynamic stability, recovering from perturbations without the equivalent of extensive "neural" feedback.

In the present study, we tested whether a simple data-driven, six-legged model with differential leg function can run effectively. As described above, our hexapedal models with large lateral and opposing leg forces show stable forward running over a range of velocities, and as we now show, they also predict constraints on fundamental gait variables and suggest that the cost of running with a sprawled posture is reduced because joint moments are minimized.

4.1 Stability with differential leg function

Our notion of effective legged locomotion is biased by our familiarity with large upright-posture bipeds and quadrupeds. In birds and mammals, legs tend to function in a similar way during symmetrical gaits. Each leg operates in the sagittal plane to store and return energy as a spring (Cavagna et al. 1977). Stability in pitch is critical (Herr et al. 2002; Lee et al. 1999). Lateral leg forces

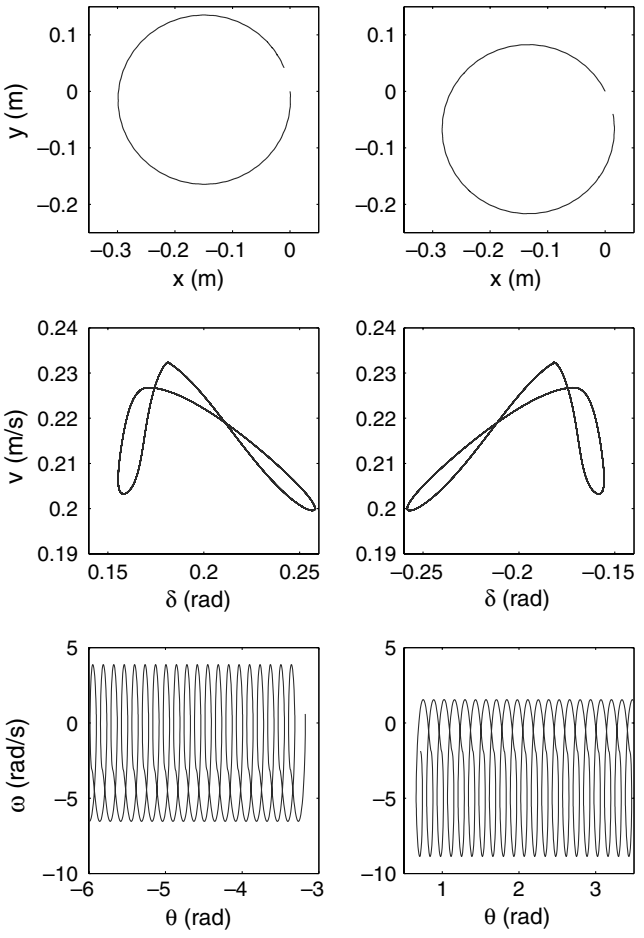

Fig. 12. Symmetry breaking: running in circles. Two attractors, symmetric under reflection, exist in the speed range in which the straight gait is unstable. *Top panels* show (x, y) spatial COM path; *middle panels* show COM speed (v)/COM velocity angle (δ) phase planes; *bottom panels* show yaw angle/angular velocity (θ, ω) phase planes to illustrate slow drift in heading: θ varies quasiperiodically with recurrence times greater than 20 full strides

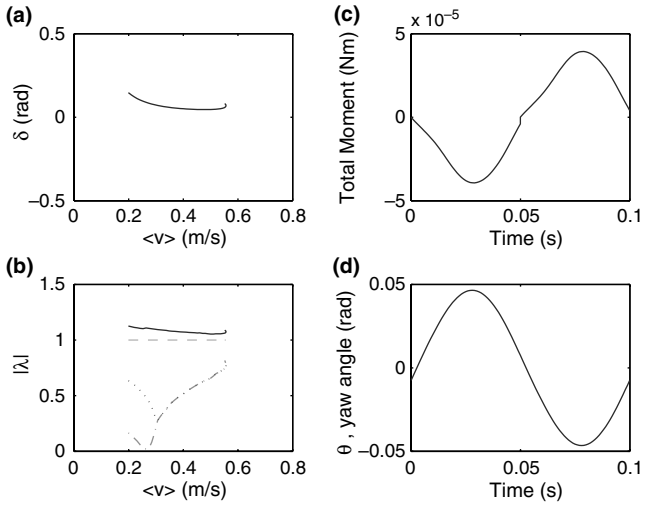

Fig. 13. Gait characteristics for a modified "upright-posture" model in which all legs exert decelerating followed by accelerating forces in the fore–aft direction, as described in Sect. 4.1. **a, b** COM velocity angle δ and eigenvalue magnitudes of linearized Poincaré map vs. "true" forward speed $< v >$. **c, d** COM moment and yaw angle (θ) variations for a full L-R stride at 0.25 cm/s^{-1}. Note instability (one eigenvalue exceeds unity) and incorrect yawing dynamics: a sine wave emerges (*bottom right*) in contrast to the cosine wave in the data of Fig. 8 (*bottom left*)

are small and opposing forces are minimized. In general the criteria for effective locomotion proposed for legged robots is met: zero horizontal foot-force interaction (Waldron 1986). Sprawled-posture runners with differential leg function have been argued to be less effective since they do not meet these criteria (Full 1993). As we now describe, the stability studies of Sect. 3 challenge this argument, and, in addition, we may capitalize on our modeling approach to ask whether a six-legged runner could be stable if it used *all* its legs like an upright-posture runner.

In spite of their stability in the saggital plane, potentially catastrophic instability in the horizontal plane is possible in sprawled-posture runners, for unrecoverable perturbations in velocity magnitude or direction can leave them vulnerable to predators. As described above, with inputs to each support tripod tailored to match the six foot-force components measured in the animal (Ting et al. 1994, Fig. 3), this led to qualitatively realistic gaits but did not *ensure* stability (recall that in solving for inputs, we neglected rotational coupling, while our dynamical model has fully coupled planar motions). Nonetheless, the hexapedal model with differential leg function is asymptotically stable at its preferred forward speed in fore–aft, lateral, and yawing velocities and (necessarily) neutrally stable in heading angle θ (Fig. 7). Forces, velocities, moments, and yaw were remarkably similar to the data collected or calculated for direct measurements on running cockroaches (Fig. 8). When we perturbed the state variables by 50%, the model retuned to a stable limit cycle in internal body coordinates (Figs. 9 and 10). Despite the fact that legs generated large lateral and opposing leg forces, the hexapedal model is stable in the horizontal plane without feedback from the external environment.

Stability with differential leg function raises the question of whether sprawled-posture runners would be stable in the horizontal plane if the legs functioned more like those of upright-posture, trotting quadrupeds (Biewener 2003, pp. 47–48). To test this hypothesis, we made each model leg act more like a passive spring in the sagittal plane, generating deceleration followed by acceleration in the fore–aft direction. We set the peak magnitudes of the front and hind leg fore–aft forces to one third those measured for the middle leg and retained the measured lateral ground reaction forces, reasoning that any other pattern would be difficult to attain given the sprawled posture. Recomputing the inputs $d_i(t), l_i(t)$ from this adjusted data, we found that this "upright-posture" model was *not necessarily stable* (Fig. 13), although we only investigated a small parameter range and we did locate a marginally stable branch with forward speeds significantly (50%) higher than design speeds (not shown). Moreover, due to the differing fore–aft force patterns, COM moments and yawing dynamics were unlike those observed in the insect. Hence, unexpectedly, the pattern viewed as effective in the sagittal plane can be unstable in the horizontal plane when used by a sprawled-posture runner.

4.2 Stability constraints on stride length and frequency

Remarkably general patterns of fundamental gait parameters have been discovered in legged animals as they increase speed (Alexander and Jayes 1983). We used our hexapedal model to test if horizontal plane stability might explain changes in two such parameters: stride length and frequency. As in Sect. 4.1, we used our modeling approach to investigate stability using both actual data and patterns not observed in the animal.

Trotting mammals, lizards, crabs, and cockroaches increase speed at lower speeds primarily by raising stride frequency, which then attains a maximum (Full 1989). Faster speeds (e.g., during galloping) are achieved by longer strides. In quadrupedal mammals both the maximum sustainable stride frequency and the speed at which it is attained scale with body mass (Heglund and Taylor 1988). A 30-g mouse changes from a trot to a gallop at a frequency twice that of a 9-kg dog, but at speeds one quarter as fast. Surprisingly, 3-g cockroaches and 30-g (eight-legged) crabs follow the same trend, suggesting the possibility of equivalent gaits in very different morphological designs. Many explanations of gait changes have been advanced. These include attaining high peak muscle stresses (Farley and Taylor 1991; Taylor 1978, 1985) or bone strains (Biewener and Taylor 1986), minimizing metabolic costs (Hoyt and Taylor 1981), scaling by dynamic similarity (Alexander 1989; Alexander and Jayes 1983), and the dynamic stability of oscillator kinematic models (Schoner et al. 1990; Vilensky et al. 1991; Collins and Stewart 1993; Golubitsky et al. 1999). Herr et al. (2002) produced pitch and forward-speed stability in dynamic quadrupedal models during trotting and galloping. We contend that the nature and generality of these relationships points to the importance of stability as a determinant of gait patterns.

Our hexapedal model supports the proposition that dynamic stability in the horizontal plane can shape the relationships of stride length and frequency with speed. It predicts that, if an animal used its preferred leg frequency across its whole speed range, it would be unstable at low speeds (Fig. 11c). An increase in stride frequency with speed provided stability at low speeds, but the resulting gaits became unstable or grazed the stability boundary near the speed at which cockroaches attain their maximum stride frequency (Fig. 11g,k). Figure 14 expands upon these data by showing stability boundaries throughout the speed–stride frequency plane and reveals that the insect's actual strategy – increasing frequency up to 30–35 cm/s^{-1} and thereafter increasing stride length as in column IV of Fig. 11 – allows it to remain within the stable "channel". Note that the solid boundaries and shaded unstable regions of Fig. 14 were computed by varying V_{des} and Ω over a grid of values *without* changing the preferred speed touchdown data of Table 1 and still indicates a path of gaits grazing the stability boundary (cf. Fig. 11k). When foot touchdown positions are modified as described in Sect. 3.2 to approximate increased stride lengths at higher speeds, the upper stability boundary moves further out and a reasonable stability margin is obtained throughout (cf. Fig. 11o).

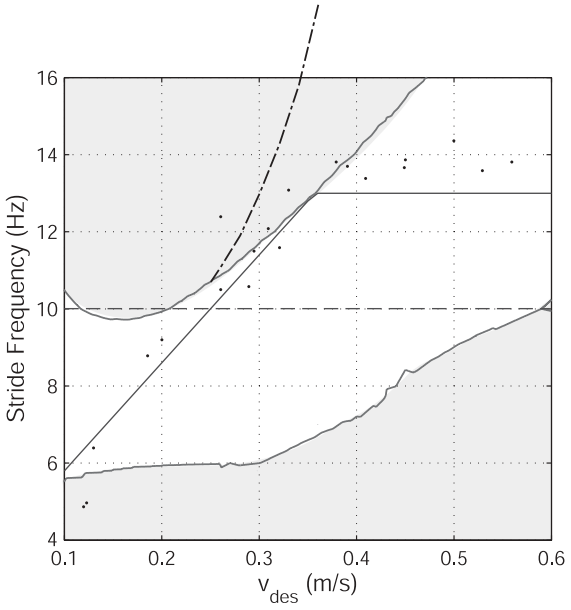

Fig. 14. A bifurcation set in desired speed-leg cycle frequency space, showing boundaries of the region in which stable gaits exist and the frequency protocols of Sect. 3.2. Unstable regions are *shaded*. Note that the fixed frequency protocol (*dashed*) encounters instability at low and/or high V_{des}, while the piecewise-linear protocol (*solid*) remains in the stable region, albeit grazing the stability boundary at its breakpoint. Stability is further improved by adjusting foot placements in this region, as described in Sect. 3.2, and shown by *dash-dotted* upper boundary above $V_{\mathrm{des}} = 0.25$. Small *dots* are data from Ting et al. (1994)

It is noteworthy that stride frequency and length must be simultaneously adjusted to maximize the stable speed range. These results suggest that the analogs of input parameters in the animal are also varied in concert, presumably by CPG feedforward-type "programs", to maintain intrinsically stable motions. This is entirely in line with the preflex hypothesis of a "neurally tuned" musculoskeletal system (Brown and Loeb 2000).

4.3 Stability with joint moment minimization

Sections 4.1 and 4.2 establish that the opposing forces generated by the cockroach support tripod provide directional stability, and that they may even be *necessary* for it (Fig. 13). We now use the model results to argue that such opposing forces confer an additional advantage on sprawled-posture animals: they tend to minimize overall joint moments.

Historically, running with an upright posture has been thought to be more effective, in part because vertically directed ground reaction forces are aligned along the limb, thereby minimizing joint moments. Vertically directed ground reaction forces in sprawled-posture animals would necessarily result in large joint moments, particularly at the "hip". However, sprawled-posture animals do not generate purely vertical ground reaction forces during running: legs push against each another, approximately aligning the force vector along the limbs as in upright-posture runners (Full 1993). Thus, fore–aft and lateral ground forces that account for most of the mechan-

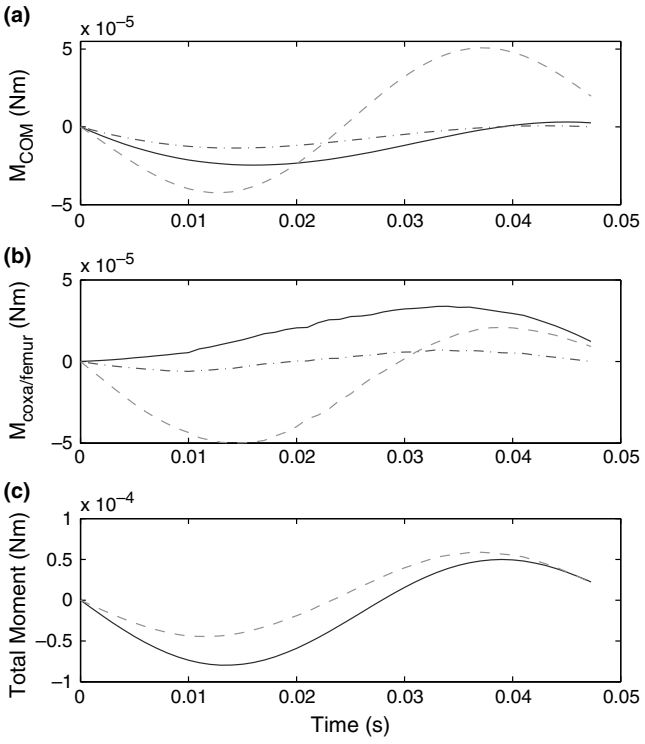

Fig. 15. Individual moments generated by the legs of the left support tripod, (**a**) at center of mass (COM) and (**b**) at coxa–femur joint: front leg *solid*, middle leg *dashed*, hind leg *chain dashed*. **c** Total moments at COM (*solid*) and coxa–femur joint (*dashed*)

ical work generated during locomotion can *reduce* total muscle force by directing ground reaction forces toward joint centers of rotation. Locomotion in sprawled-posture animals such as insects, centipedes, and lizards does not necessarily result in large moments at joints or large muscle forces. This is consistent with the finding that minimum metabolic costs of locomotion in species that differ in posture can be similar (Full 1989).

Our model reveals that fore and hind legs require small moments (d_i magnitudes) to produce the ground reaction forces observed in running cockroaches (Fig. 6). Moments generated by middle legs are nearly twice as large, but comparison with measurements from the coxa–femur joint in cockroaches reveals that even these larger moments are less than 10% of the maximum moments that animals can produce (Full and Ahn 1995). However, minimization of joint moments near the body does not imply that ground reaction forces are directed through all joint centers of rotation: bent multisegment legs make this impossible. Full et al. (1991) tested the hypothesis that deviations from the minimum moments in running cockroaches could be explained by considering the minimization of the summed muscle forces in several legs. Calculations demonstrated that measured ground reaction forces in the sagittal plane were within 12% of that which would minimize muscle forces.

Plotting the present hexapedal model's individual leg moments about the approximate position of coxa–femur joints and the COM reveals that the legs of each tripod produce moment patterns that sum to rotate the body with little cancellation: indeed, the front and rear leg COM moments oppose the middle one only in the third quarter of the stance phase (Fig. 15(a)). This also reveals why d_2, the middle leg moment arm, moves in the opposite direction to the front and hind moment arms (Fig. 6): to produce similar COM moments from all three support legs. Hence the inwardly directed opposing leg forces do *not* generate substantial opposing moments, and, given that nonzero net COM moments are observed, they are thereby produced in an efficient manner.

To further investigate the role of moments, a study was conducted in which the "design" hip position inputs $d_i(t)$ used in the fourth protocol of Fig. 11 were perturbed in a manner that preserves the net COM moments but changes individual leg moments. Specifically, we shifted d_1, d_4 (the front pivot positions) forward on the body by 0.1–0.3 cm and d_3, d_6 (back pivot positions) backward by 0.1–0.3 cm, leaving the middle pivot positions d_2, d_5 alone. This significantly increased front leg coxa–femur moments, slightly increased rear leg moments, and led to substantial cancellation of opposing front and rear moments. More significantly, *all* the resulting perturbed gaits had one eigenvalue of magnitude greater than one, and so were unstable (data not shown). Leg actions that minimize individual coxa–femur moments also appear necessary for passive stability!

We may ask why nonzero moments are necessary at all for straight running or, equivalently, why animals exhibit appreciable yawing motions. If all model hips are fixed at the COM ($d_i \equiv 0$), then rotation decouples completely and moments are zero, and in principle nonzero moments could be produced by reflexive feedback only when needed to correct yaw perturbations (recall the comments at the end of Sect. 3.2). Rapid force sensor (campaniform sensilla) reflexes (Höltje and Hustert 2003) imply that this is possible in stereotyped movements, but the delays in controlled muscle force generation, estimated at 25–30 ms in Jindrich and Full (2002), suggest that it may be harder to produce precise control "on demand" within a step. Moreover, Jindrich and Full (2002) discovered that the moments necessary to produce large turns in insects required only minor alterations in forces generated in stable, straight-ahead locomotion (Jindrich and Full 1999), and we have confirmed that this is also possible via small d-variations in the LLS model (Schmitt and Holmes 2000b). Hence, laterally opposing leg forces, generally perceived to be ineffective, may actually work synergistically to enhance stability and maneuverability. Perhaps the energetic costs of locomotion balance the stability and increases in muscle force production.

5 Conclusions

The Kubow and Full (1999), Schmitt and Holmes (2000a,b), and Schmitt et al. (2002) models represent opposite extremes; in Kubow and Full (1999), foot forces are completely prescribed and do not respond to perturbations; in Schmitt and Holmes (2000a,b); Schmitt et al. (2002), they are entirely determined by the body motions,

and hence respond immediately to perturbations. Force measurements in response to momentum perturbations show changes in lateral velocity of $0.2\,\mathrm{ms}^{-1}$ occurring within 15 ms (Jindrich and Full 2002, Fig. 3), corresponding to forces of 0.3–0.4 N, two orders of magnitude greater than the lateral forces typical of unperturbed running (Fig. 8). At the same time, changes in the number and phasing of motoneuron action potentials directly affect muscle forces (Full et al. 1998). Hence, neither purely prescribed nor purely passive forces adequately represent the situation. Along with Schmitt and Holmes (2003), the present paper develops a model in which, as in the insect, forces are partially prescribed in a feedforward manner and partially determined by mechanical (preflex) feedback due to interaction with the environment. As we have noted, this is a step toward an integrated neuromechanical model of a behaving animal.

The dynamics of the hexapedal lateral leg spring model developed here compares well with insect body dynamics (Fig. 8). Furthermore, the model exhibits stable trajectories for a range of velocities typical of the animal (Figs. 11 and 14). Four cases were considered. In the first, the desired forward speed V_{des} alone changes, and we retain constant leg cycle frequency, so that faster running is achieved by taking longer strides. In the second, leg cycle frequency Ω increases linearly, and in the third it increases up to a transition speed, after which it remains constant. In the fourth case, foot touchdown positions $\mathbf{b}_j$ are also adjusted in a manner suggested by insect data, to increase stride length and maintain approximate symmetry by keeping the COM near the center of the support triangle at midstride.

The latter two protocols exhibit improved stability characteristics, due jointly to the more natural frequency and foot placement variations, but such hypotheses cannot be tested in detail until precise relationships between directly measureable insect and model parameters are known over the whole speed range. Moreover, earlier studies (Schmitt and Holmes 2001; Schmitt et al. 2002) and numerical simulations of the current model not reported here reveal that gait stability depends on several parameters in addition to speed, stride frequency, and foot placement points; for example, moment of inertia I and spring constant k play important roles. Future work will require development of more realistic leg-muscle models and more exhaustive parameter studies, perhaps using nondimensional quantities and scaling relations, as in Schmitt and Holmes (2001).

The present model further weakens the hypothesis that sprawled-posture, polypedal locomotion is less effective than upright posture running with fewer legs. Sprawled-posture runners are stable in both the sagittal and horizontal planes over a range of speeds. Stability with differential leg function does not appear to be compromised by large joint moments during running because leg ground reaction forces are aligned along the leg directed toward the COM, and moments due to individual legs cooperate to produce the net turning moments that sustain the insect's stable weaving trajectory (Fig. 15). Legs radiating out in all directions with the capability of generating large moments may allow very rapid turning and other extraordinary maneuvers.

Acknowledgements. This work was supported by DARPA/ONR: N00014-98-1-0747 and DoE: DE-FG02-95ER25238. Justin Seipel was supported by an NSF Graduate Fellowship.

Appendix

Computational and analytical details

Numerical approximation of eigenvalues A forward-difference algorithm was used to numerically calculate eigenvalues of the Jacobian of the Poincaré return map (15). First a fixed point of the map

$$\mathbf{P}(\mathbf{x}^*) = \mathbf{x}^* \tag{16}$$

was approximated using a nonlinear least-squares algorithm. Then each of the state variable values $\mathbf{x} = (v, \delta, \theta, \omega)$ were in turn perturbed by a small amount Δx_j. For a perturbation in the jth element of the state vector, the jth column of the Jacobian of the map is approximated by the following equation:

$$\frac{\partial \mathbf{P}}{\partial x_j} \approx \frac{\mathbf{P}(\mathbf{x}^* + \Delta x_j \mathbf{e}_j) - \mathbf{P}(\mathbf{x}^*)}{\Delta x_j}\,. \tag{17}$$

We found that requiring errors less than 10^{-4} sufficed in the nonlinear least-squares scheme implemented in Matlab by the `fsolve` function, using its medium-scale, trust-region dogleg method (a variant of the Powell dogleg method, Powell 1970). The numerical routine was checked using a damped harmonic oscillator with a known analytic solution: agreement was excellent.

Touchdown protocol details for high-speed range

For the final set of variable-speed data presented in column IV of Fig 11, we adjusted foot touchdown positions for the left tripod for $V_{\mathrm{des}} > 0.25\,\mathrm{m\,sec}^{-1}$ as follows (right tripod touchdown positions follow via reflection about the body axis):

$$\begin{aligned}
\mathbf{b}_{1,e1}(V_{\mathrm{des}}) &= \mathbf{b}_{1,e1} + 0.02(V_{\mathrm{des}} - 0.25)\,,\\
\mathbf{b}_{1,e2}(V_{\mathrm{des}}) &= \mathbf{b}_{1,e2} + 0.04(V_{\mathrm{des}} - 0.25)\,,\\
\mathbf{b}_{2,e1}(V_{\mathrm{des}}) &= \mathbf{b}_{2,e1} - 0.02(V_{\mathrm{des}} - 0.25)\,,\\
\mathbf{b}_{2,e2}(V_{\mathrm{des}}) &= \mathbf{b}_{2,e2} + 0.04(V_{\mathrm{des}} - 0.25)\,,\\
\mathbf{b}_{3,e1}(V_{\mathrm{des}}) &= \mathbf{b}_{3,e1} - 0.02(V_{\mathrm{des}} - 0.25)\,,\\
\mathbf{b}_{3,e2}(V_{\mathrm{des}}) &= \mathbf{b}_{3,e2} + 0.03(V_{\mathrm{des}} - 0.25)\,.
\end{aligned}$$

Here $\mathbf{b}_j$ denote the nominal touchdown vectors specified in Table 1, and $\mathbf{b}_j(V_{\mathrm{des}})$ denote the modified placements. Note that dependence on V_{des} is linear and that legs are extended and swung further forward as V_{des} increases. This parallels the decrease in touchdown angle β and increase in relaxed leg length l adopted in (Schmitt et al. 2002, Sect. 4.4), and, as noted in the text, it effectively limits leg-length increases to within 50% above those at preferred speed.

References

Alexander NMcR (1989) Optimisation and gaits in the locomotion of vertebrates. Physiol Rev 69:1199–1227

Alexander NMcR, Jayes AS (1983) A dynamic similarity hypothesis for the gaits of quadrupedal maammals. J Zool Lond 201:135–152

Biewener AA (2003) Animal locomotion. Oxford University, Oxford

Biewener AA, Taylor CR (1986) Bone strain: a determinant of gait and speed? J Exp Biol 123:383–400

Blickhan R (1989) The spring-mass model for running and hopping. J Biomech 11/12:1217–1227

Blickhan R, Full RJ (1993) Similarity in multi-legged locomotion: bouncing like a monopode. J Comp Physiol A 173:509–517

Brown IE, Loeb GE (2000) A reductionist approach to creating and using neuromusculoskeletalmovement. In: Winters MJ, Crago EP (eds) Biomechanics and neural control of movement. Springer, Berlin Heidelberg New York, pp 148–163

Brown IE, Scott SH, Loeb GE (1995) "Preflexes" – programmable high-gain zero-delay intrinsic responses of perturbed musculoskeletal systems. Soc Neurosci Abstr 21:562.9

Cavagna GA, Heglund NC, Taylor CR (1977) Mechanical work in terrestrial locomotion: two basic mechanismsfor minimizing energy expenditure. Am J Physiol 233(5):R243–R261

Chong L, Culotta E, Sugden A (eds) (2000) On the move: Movement: molecular to robotic. Science 288:79–106

Collins JJ, Stewart I (1993) Hexapodal gaits and coupled nonlinear oscillator models. Biol Cybern 68(4):287–298

Dickinson MH, Farley CT, Full RJ, Koehl MAR, Kram R, Lehman S (2000) How animals move: an integrative view. Science 288:100–106

Farley CT, Taylor CR (1991) A mechanical trigger for the trot-gallop transition in horses. Science 253:306–308

Full RJ (1989) Mechanics and energetics of terrestrial locomotion: from bipeds to polypeds. In: Weiser W, Gnaiger E (eds) Energy transformation in cells and animals. Georg Thieme, Stuttgart, pp 175–182

Full RJ (1993) Integration of individual leg dynamics with whole body movement in arthropod locomotion. In: Beer R, Ritzmann R, McKenna T (eds) Biological neural networks in invertebrate neuroethology and robots. Academic, Boston, pp 3–20

Full RJ, Ahn AN (1995) Static forces and moments generated in the insect leg: comparison of a three-dimensional musculo-skeletal computer model with experimental measurements. J Exp Biol 198:1285–1298

Full RJ, Koditschek DE (1999) Templates and anchors: neuromechanical hypotheses of legged locomotion on land. J Exp Biol 202:3325–3332

Full RJ, Tu MS (1990) Mechanics of six-legged runners. J Exp Biol 148:129–146

Full RJ, Tu MS (1991) Mechanics of a rapid running insect: two-four- and six-legged locomotion. J Exp Biol 156:215–231

Full RJ, Blickhan R, Ting LH (1991) Leg design in hexpedal runners. J Exp Biol 158:369–390

Full RJ, Stokes D, Ahn AN, Josephson RK (1998) Energy absorption during running by leg muscles in a cockroach. J Exp Biol 201:997–1012

Full RJ, Kubow T, Schmitt J, Holmes P, Koditschek D (2002) Quantifying dynamic stability and maneuverability in legged locomotion. Integ Comp Biol 42:149–157

Golubitsky M, Stewart I, Buono PL, Collins JJ (1999) Symmetry in locmotor central pattern generators and animal gaits. Nature 401:693–695

Guckenheimer J, Holmes P (1990) Nonlinear oscillations dynamical systems and bifurcations of vector fields. Springer, Berlin Heidelberg New York

Guckenheimer J, Johnson S (1995) Planar hybrid systems. Lecture notes in computer science, vol 999. Springer, Berlin Heidelberg New York

Heglund NC, Taylor CR (1988) Speed stride frequency and energy cost per stride. How do they change with body size and gait? J Exp Biol 138:301–318

Herr H, Huang GT, McMahon TA (2002) A model of scale effects in mammalian quadrupedal running. J Exp Biol 205:959–967

Höltje M, Hustert R (2003) Rapid mechano-sensory pathways code leg impact and elicit very rapid reflexes in insects. J Exp Biol 206:2715–2724

Hoyt DF, Taylor CR (1981) Gait and the energetics of locomotion in horses. Nature 292:239–240

Jindrich D, Full RJ (1999) Many-legged maneuverability: dynamics of turning in hexapods. J Exp Biol 202:1603–1623

Jindrich D, Full RJ (2002) Dynamic stabilization of rapid hexapedal locomotion. J Exp Biol 205:2803–2823

Kram R, Wong B, Full RJ (1997) Three-dimensional kinematics and limb kinetic energy of running cockroaches. J Exp Biol 200:1919–1929

Kubow TM, Full RJ (1999) The role of the mechanical system in control: a hypothesis of self-stabilization in hexapedal runners. Philos Trans R Soc Lond B 354:849–861

Lee DV, Bertram JEJ, Todhunter RJ (1999) Acceleration and balance in trotting dogs. J Exp Biol 202:3565–3573

Maddocks J (1984) Stability of nonlinearly elastic rods. Arch Rat Mech Anal 85:311–354

Maddocks J (1987) Stability and folds. Arch Rat Mech Anal 99:301–328

McMahon TA, Cheng GC (1990) The mechanics of running: how does stiffness couple with speed? J Biomech 23(suppl 1):65–78

Powell MJD (1970) A Fortran subroutine for solving systems of nonlinear algebraic equations. In: Rabinowitz P (ed) Numerical methods for nonlinear algebraic equations. Gordon and Breach, London, pp 115–161

Ruina A (1998) Non-holonomic stability aspects of piecewise holonomic systems. Rep Math Phys 42(1/2):91–100

Schmitt J, Holmes P (2000a) Mechanical models for insect locomotion: dynamics and stability in the horizontal plane – theory. Biol Cybern 83(6):501–515

Schmitt J, Holmes P (2000b) Mechanical models for insect locomotion: dynamics and stability in the horizontal plane – application. Biol Cybern 83(6):517–527

Schmitt J, Holmes P (2001) Mechanical models for insect locomotion: stability and parameter studies. Physica D 156(1–2): 139–168

Schmitt J, Holmes P (2003) Mechanical models for insect locomotion: active muscles and energy losses. Biol Cybern 89(1):43–55

Schmitt J, Garcia M, Razo CR, Holmes P, Full RJ (2002) Dynamics and stability of legged locomotion in the horizontal plane: a test case using insects. Biol Cybern 86(5):343–353

Schoner G, Jiang WY, Kelso JA (1990) A synergetic theory of quadrupedal gaits and gait transitions. J Theor Biol 142:359–391

Taylor CR (1978) Why change gaits? Recruitment of muscles and muscle fibers as a function of speed and gait. Am Zool 18:153–161

Taylor CR (1985) Force development during sustained locmotion: a determinant of gait speed and metabolic power. J Exp Biol 115:253–262

Ting LH, Blickhan R, Full RJ (1994) Dynamic and static stability in hexapedal runners. J Exp Biol 197:251–269

Vilensky JA, Libii JN, Morre M (1991) Trot-gallop gait transitions in quadrupeds. Physiol Behav 50:835–842

Waldron KJ (1986) Force and motion management in legged locomotion. IEEE J Robot Automat RA-2(4):214–220